

RESEARCH ARTICLE

Therapeutic effects of lisinopril and empagliflozin in a mouse model of hypertension-accelerated diabetic kidney disease

✉ Mette V. Østergaard, Thomas Secher, Michael Christensen, Casper Gravesen Salinas, Urmas Roostalu, Jacob Lercke Skytte, Ida Rune, ✉ Henrik H. Hansen, Jacob Jelsing, Niels Vrang, and Lisbeth N. Fink
Gubra Aps, Horsholm, Denmark

Abstract

Hypertension is a critical comorbidity for progression of diabetic kidney disease (DKD). To facilitate the development of novel therapeutic interventions with the potential to control disease progression, there is a need to establish translational animal models that predict treatment effects in human DKD. The present study aimed to characterize renal disease and outcomes of standard of medical care in a model of advanced DKD facilitated by adeno-associated virus (AAV)-mediated renin overexpression in uninephrectomized (UNx) *db/db* mice. Five weeks after single AAV administration and 4 wk after UNx, female *db/db* UNx-ReninAAV mice received (PO, QD) vehicle, lisinopril (40 mg/kg), empagliflozin (20 mg/kg), or combination treatment for 12 wk ($n = 17$ mice/group). Untreated *db/+* mice ($n = 8$) and vehicle-dosed *db/db* UNx-LacZAAV mice ($n = 17$) served as controls. End points included plasma, urine, and histomorphometric markers of kidney disease. Total glomerular numbers and individual glomerular volume were evaluated by whole kidney three-dimensional imaging analysis. *db/db* UNx-ReninAAV mice developed hallmarks of progressive DKD characterized by severe albuminuria, advanced glomerulosclerosis, and glomerular hypertrophy. Lisinopril significantly improved albuminuria, glomerulosclerosis, tubulointerstitial injury, and inflammation. Although empagliflozin alone had no therapeutic effect on renal endpoints, lisinopril and empagliflozin exerted synergistic effects on renal histological outcomes. In conclusion, the *db/db* UNx-ReninAAV mouse demonstrates good clinical translatability with respect to physiological and histological hallmarks of progressive DKD. The efficacy of standard of care to control hypertension and hyperglycemia provides a proof of concept for testing novel drug therapies in the model.

NEW & NOTEWORTHY Translational animal models of diabetic kidney disease (DKD) are important tools in preclinical research and drug discovery. Here, we show that the standard of care to control hypertension (lisinopril) and hyperglycemia (empagliflozin) improves physiological and histopathological hallmarks of kidney disease in a mouse model of hypertension-accelerated progressive DKD. The findings substantiate hypertension and type 2 diabetes as essential factors in driving DKD progression and provide a proof of concept for probing novel drugs for potential nephroprotective efficacy in this model.

ACE inhibitor; diabetic kidney disease; glomerulosclerosis; mouse model; SGLT2 inhibitor

INTRODUCTION

Diabetes is the leading cause of chronic kidney disease (CKD) globally, accounting for nearly half of all cases of end-stage kidney disease (ESKD). Approximately 40% of patients with type 2 diabetes (T2D) develop CKD, and the prevalence is predicted to increase to around 50% by 2025 (1, 2). The progression of diabetic kidney disease (DKD) is characterized by progressive albuminuria and declining glomerular filtration rate (GFR), concomitant with cardiovascular disease and ultimately ESKD. The pathophysiology of DKD involves an interplay of metabolic and hemodynamic factors (3), and thus control of blood glucose and blood pressure has been the cornerstone in DKD risk management and treatment for the last two decades. Renin-angiotensin-aldosterone system (RAAS) blockade using angiotensin-converting enzyme

(ACE) inhibitors and angiotensin II receptor antagonists represents the standard of medical care for hypertension control and improves both renal and cardiovascular outcomes in patients with T2D and DKD (4–6). Of the new antidiabetic drug classes, sodium-glucose cotransporter-2 (SGLT2) inhibitors are of particular interest for DKD management. Recent clinical trials have demonstrated that SGLT2 inhibition, when added to RAAS blockade, slows the rate of GFR decline and lowers the risk for ESKD and death from cardiovascular causes in patients with DKD (7). Notably, SGLT2 inhibitors may have nephroprotective effects independent of their glucose-regulatory action, as the benefits of dual RAAS and SGLT2 inhibition also extend to patients with CKD without diabetes (7–10).

Despite the recent improvement of CKD care in diabetes, the prevalence of DKD remains high among patients with

T2D, and improved treatment modalities to prevent DKD progression are urgently required. Consequently, there is a need for animal models that more closely resemble the multifactorial features of the human disease to better predict clinical treatment responses. To reflect recent advances in DKD treatment, preclinical efficacy testing of potential DKD therapeutics should be conducted in the context of concurrent RAAS blockade and SGLT2 inhibitor treatment.

Induction of persistent hypertension by adeno-associated virus (AAV)-mediated renin gene transfer has recently been reported to exacerbate kidney injury in uninephrectomized (UNx) *db/db* mice (11, 12). Because the *db/db* UNx-ReninAAV mouse shows close resemblance to human DKD pathogenesis (12), we further validated the model for utility in preclinical drug discovery by characterizing renal disease and outcomes of the long-term standard of care using an ACE inhibitor (lisinopril) and SGLT2 inhibitor (empagliflozin).

METHODS

Animals

The Danish Animal Experiments Inspectorate approved all experiments, which were conducted using internationally accepted principles for the use of laboratory animals (License No. 2013-15-2934-00784). Female *db/m* and *db/db* (BKS.Cg-Dock7m+/+Leprdb/J) mice (5-wk-old) were obtained from Charles River (Calco, Italy) and housed in a controlled environment (12:12-h light-dark cycle, lights on at 3 AM, 23 ± 2°C, humidity: 50 ± 10%). Female *db/db* mice are less prone to develop hydronephrosis and pyelonephritis with increasing age compared with male *db/db* mice (13–15). Each animal was identified by an implantable subcutaneous microchip (PetID Microchip, E-vet, Haderslev, Denmark). Mice had ad libitum access to standard chow (Altromin 1324, Brogaarden, Hørsholm, Denmark) and tap water.

UNx and AAV Delivery of Renin

An AAV construct, AAV8-TBG-m-Ren1d(F61R/P65S), was used to induce hypertension (16). An AAV8-TBG-LacZ construct expressing LacZ was used as the negative control. Both constructs are expressed under the control of the liver-specific thyroxin-binding globulin promoter (12, 17). ReninAAV and LacZAAV were from Vector Biolabs (Malvern, PA). Animals were randomized according to baseline fed blood glucose and body weight 1 wk before AAV administration. AAV constructs were suspended in sterile PBS and administered by tail vein injection in conscious animals (7 wk of age). In an initial dose-finding study in *db/db* UNx mice ($n = 10$ – 13 mice/group), ReninAAV doses of 1×10^{10} , 2×10^{10} , 4×10^{10} , and 10×10^{10} genome copies (GC) were characterized and compared with LacZ 2×10^{10} GC (see the study outline provided in Supplemental Fig. S1; all Supplemental Material available at <https://doi.org/10.6084/m9.figshare.14431229.v1>). One week after AAV injection, UNx was performed as previously described (14). Animals were allowed to recover for 4 wk before the study start (defined as *week 1*). Body weight was measured twice a week from 1 wk before AAV administration until the study start and thereafter once daily. Mice were euthanized 12 wk after the study start, corresponding to 17 wk after AAV administration.

Drug Treatment

In a subsequent intervention study, a ReninAAV and LacZAAV dose of 2×10^{10} GC was used (see the study outline in Supplemental Fig. S1). Treatment was initiated 5 wk after AAV administration. Randomization and stratification to treatment were based on fed blood glucose and body weight measured 2 days before the treatment start. *db/db* UNx-ReninAAV mice ($n = 17$ mice/group) received (PO, QD) vehicle (0.5% methyl cellulose), lisinopril (40 mg/kg, MedChemExpress, Monmouth Junction, NJ), empagliflozin (20 mg/kg, MedChemExpress), or lisinopril + empagliflozin (40 mg/kg + 20 mg/kg) for 12 wk. Untreated female *db/m* mice ($n = 8$) and vehicle-dosed *db/db* UNx-LacZAAV mice ($n = 15$) served as controls. Doses of lisinopril and empagliflozin were within standard ranges used for mouse models of DKD (18).

Blood Pressure

In the ReninAAV dose-finding study, systolic arterial blood pressure was measured on *weeks 4* and *10* by tail-cuff plethysmography using a mouse tail-cuff system (IITC Life Science, Woodland Hills, CA). Animals were randomly selected for blood pressure measurement and trained in the system for 4 consecutive days before blood pressure measurement on the fifth day.

Transcutaneous FITC-Sinistrin Measurement

GFR was measured in the ReninAAV dose-finding study by FITC-sinistrin clearance in *week 10*. The GFR monitor (MediBeacon, Mannheim, Germany) was mounted on the back of the animal according to the manufacturer's instructions. FITC-sinistrin was injected into the tail vein (40 mg/mL, 0.15 mg/g body wt), and FITC-sinistrin was monitored transcutaneously for up to 90 min postinjection in conscious and freely moving animals. GFR in $\mu\text{L}/\text{min}/100$ g body wt was estimated using MDP Studio software (MediBeacon, St. Louis, MO) using a conversion factor to express GFR in $\mu\text{L}/\text{min}$ (19).

Blood and Urine Analyses

Blood and urine samples were collected from nonfasted animals. Tail blood samples were collected every 3–4 wk. Spot urine samples were collected in *weeks 6* and *12* (ReninAAV dose-finding study) or *week 11* (treatment study). Blood glucose, glycated hemoglobin A1c (HbA1c), plasma urea, urine albumin, and creatinine were determined as previously described (14). Terminal plasma cystatin C levels were determined using an ELISA kit (R&D Systems, Minneapolis, MN).

Histology

Histology was performed on sections from formalin-fixed (conventional histology) or glyoxal-fixed [three-dimensional (3D) imaging and conventional histology] kidneys as previously described in detail (14, 20). All histological analyses were performed on cleared kidneys as described below in *Whole Kidney Quantitative 3D Imaging Analysis of Glomeruli Number and Volume*. Stained sections were scanned with a $\times 20$ objective using a Scanscope AT slide scanner (Aperio, Leica Biosystems, Buffalo Grove, IL), and quantitative image analysis was performed using Visiopharm software (Visiopharm,

Hørsholm, Denmark). Collagen type III (no. 1330-01, SouthernBiotech, Birmingham, AL) and CD1b (ab133357, Abcam, Cambridge, UK) was quantified in the renal cortex, whereas kidney injury molecule-1 (KIM-1; AF1817, R&D Systems) was quantified in the whole section. Data were expressed as total mass (mg) of positive staining by multiplying terminal kidney weight with the corresponding fractional (%) surface area of positive staining.

Glomerulosclerosis Scoring Using Deep Learning

In the ReninAAV dose-finding study, periodic acid-Schiff (PAS)-positive staining was determined inside glomeruli by artificial intelligence (AI)-assisted image analysis. Slides were scanned with a 20× objective. Glomerulosclerosis was quantified according to the percentage of the glomerular tuft occupied with PAS-positive and nuclei-free matrix (21, 22). Total PAS-positive staining was expressed as total mass (mg) of positive staining by multiplying terminal kidney weight with the corresponding fractional (%) surface area of positive staining. In the pharmacological study, the glomerulosclerosis score was computed by detecting all glomeruli using a neural network, whereafter each glomeruli was assigned a glomerulosclerosis score by a second neural network. A U-net network architecture (23) was trained to segment glomeruli from 2,324 annotated glomeruli derived from 20 kidneys sampled across all study groups. Network training was performed in Visiopharm Integrator Software (VIS2020.1.3, Visiopharm, Hørsholm, Denmark) using the AI module and analyzed at ×10 magnification. The trained model was evaluated by visual inspection. Glomeruli were next classified according to a five-point scale using the following criteria: GS0 (normal), GS1 (mild, sclerotic area up to 25%), GS2 (moderate, sclerotic area of 25–50%), GS3 (severe, sclerotic area of 51–75%), and GS4 (global, sclerotic area of 76–100%) with a second neural network. The training set consisted of the following number of samples (glomeruli): GS0 ($n = 943$), GS1 ($n = 970$), GS2 ($n = 960$), GS3 ($n = 725$), and GS4 ($n = 507$). An Inceptionv3 network (24) was trained using the Keras library (25) to assign glomerulosclerosis scores. Images were analyzed at ×20 magnification. The trained model had an accuracy of 66% measured on a test set of 269 samples. For both neural networks, the prediction error was measured as cross entropy, and the Adam optimizer (26) was used during training. Data augmentation, in the form of rotations, flips, and brightness, was applied. Data were expressed as the number of glomeruli with individual glomerulosclerosis scores (GS0–GS4 and GS3–GS4, respectively) relative to total glomeruli counts in the corresponding experimental group (fraction %). The glomerulosclerosis index was calculated using the following formula: $(1 \times n_1) + (2 \times n_2) + (3 \times n_3) + (4 \times n_4) / n_0 + n_1 + n_2 + n_3 + n_4$, where n_x is the number of glomeruli in each grade of glomerulosclerosis (27).

Whole Kidney Quantitative 3D Imaging Analysis of Glomeruli Number and Volume

Whole kidney 3D imaging analysis was applied in the treatment study. Procedures were according to a previous report in *db/db* UNx mice (20). In brief, anesthetized mice were injected in the tail vein with DyLight-594-conjugated *Lycopersicon esculentum* (tomato) lectin (Vector Laboratories,

Burlingame, CA), which labels endothelial cells and blood vessels, including glomerular capillaries (28). After 5 min, mice were transcardially perfused with heparinized PBS. Glyoxal-fixed kidneys were imaged by light-sheet fluorescence microscopy using a LaVision Ultramicroscope II (Miltenyi Biotec, Bergisch Gladbach, Germany). Procedures for automated mapping, segmentation, quantification, and statistical evaluation of glomeruli numbers and volumes have been previously described in detail (20). 3D segmentation of glomeruli consisted of two steps. First, a two-dimensional U-Net network architecture (28) was trained to detect glomeruli centroids, based on annotations from 291 randomly sampled image tiles (512×512 pixels). Data augmentation, in the form of rotations and nonlinear distortions, was applied during training, and detected glomeruli centroids were used as input for a seeded 3D watershed segmentation. Using the image gradients, this operation filled out the entire glomerular area around each detected centroid, resulting in the final 3D glomeruli segmentation.

Statistics

Except from quantitative 3D imaging, data were analyzed using GraphPad Prism v7.03 software (GraphPad, La Jolla, CA). All results are shown as means ± SE. Dunnett's test one-factor/two-factor linear model with interaction was used with a P value of <0.05 considered statistically significant.

RESULTS

Robust Diabetic Nephropathy in ReninAAV-Injected UNx *db/db* Mice

A single injection of ReninAAV (ReninAAV 1– 10×10^{10} GC) was evaluated for metabolic and renal effects in female *db/db* UNx mice compared with LacZAAV control mice (2×10^{10} GC). Physiological parameters are shown in Table 1 and provided in Supplemental Table S1. ReninAAV doses up to 4×10^{10} GC did not influence diabetes severity in *db/db* UNx mice (Fig. 1A). ReninAAV promoted dose-dependent increments in systolic arterial blood pressure, with doses of $\geq 2 \times 10^{10}$ GC inducing robust and persistently elevated blood pressure ($P < 0.05$ – 0.001 ; Fig. 1B). Consistent with a previous ReninAAV dose-response study in mice using the same vector and renin construct (17), the survival rate was reduced in *db/db* UNx mice that received a ReninAAV dose of $\geq 4 \times 10^{10}$ GC (Table 1), being associated with spontaneous major vessel rupture. ReninAAV 2×10^{10} GC promoted progressive elevations in the urine albumin-to-creatinine ratio (ACR; $P < 0.05$ vs. week 6; Fig. 1C). Terminal plasma cystatin C levels were only significantly elevated by high ReninAAV doses ($\geq 4 \times 10^{10}$ GC, $P < 0.05$ – 0.001 ; Fig. 1D). A ReninAAV dose-dependent decline in GFR was noted, but without attaining statistical significance ($P = 0.128$ – 0.265 ; Table 1). ReninAAV ($\geq 4 \times 10^{10}$ GC) significantly increased glomerular PAS-positive mass ($P < 0.001$; Fig. 1E). Although LacZAAV control and ReninAAV mice (1×10^{10} GC) showed mild mesangial matrix expansion, higher ReninAAV doses ($\geq 2 \times 10^{10}$ GC) promoted segmental and global glomerulosclerosis (Fig. 1F). A 2×10^{10} GC dose was used in the drug treatment study as robust elevations in blood pressure and urine ACR were obtained without any significant mortality.

Table 1. ReninAAV dose-finding study

	db/db UNx-LacZAAV ×2	db/db UNx-ReninAAV ×1	db/db UNx-ReninAAV ×2	db/db UNx-ReninAAV ×4	db/db UNx-ReninAAV ×10
Survival rate, <i>n</i>	7/10	10/12	9/13	4/12	3/12
Body weight at randomization (week 6), g	35.5 ± 0.9	36.1 ± 0.6	34.7 ± 0.6	35.0 ± 0.8	37.1 ± 2.6
Fed blood glucose at randomization (week 6), mmol/L	13.0 ± 1.7	12.2 ± 1.0	12.2 ± 1.0	12.2 ± 1.4	10.6 ± 1.6
Body weight at GFR test (week 10), g	46.7 ± 2.9	50.0 ± 1.9	49.4 ± 1.5	51.4 ± 4.0	48.3 ± 3.8
GFR (week 10), μL/min	493 ± 43	620 ± 39	415 ± 48	396 ± 42	344 ± 50
GFR relative (week 10), μL/min/100 g body wt	1,059 ± 78	1,246 ± 75	843 ± 85	768 ± 43	753 ± 34
Half-life of sinistrin, min	14.3 ± 1.1	12.1 ± 0.6	18.6 ± 1.7	19.2 ± 1.1	19.5 ± 0.9
Body weight (week 12), g	44.9 ± 3.4	47.8 ± 2.2	48.1 ± 1.5	50.7 ± 3.9	45.8 ± 2.8
Fed blood glucose (week 12), mmol/L	21.1 ± 4.9	20.6 ± 2.1	20.0 ± 2.7	13.3 ± 4.3	5.1 ± 0.2
Plasma urea (week 12), mmol/L	10.9 ± 1.8	9.5 ± 0.4	9.0 ± 0.7	11.4 ± 0.7	10.5 ± 0.6
Kidney weight (week 12), mg	368 ± 28	381 ± 13	337 ± 19	359 ± 26	294 ± 32
Relative kidney weight (week 12), mg/g body wt	8.5 ± 2.1	8.3 ± 0.6	7.1 ± 0.4	7.5 ± 1.2	6.5 ± 0.4
Heart weight (week 12), mg	200 ± 19	228 ± 14	284 ± 17†	300 ± 24†	283 ± 34
Relative heart weight (week 12), mg/g body wt	4.5 ± 0.3	4.9 ± 0.3	6.0 ± 0.3*	6.1 ± 0.5	6.3 ± 0.6

All data are presented as means ± SE; *n*, number of mice. Physiological data in diabetic *db/db* uninephrectomized (UNx) mice administered various doses of adeno-associated virus (AAV)-delivered renin and compared with LacZAAV controls are shown. AAV LacZ or renin construct was intravenously administered in study week -5 (7 wk of age), and UNx was performed in female *db/db* mice in study week -4. Mice were euthanized 17 wk after single AAV administration, corresponding to study week 12. Data are only shown from mice that completed the entire study. LacZAAV ×2, 2 × 10¹⁰ genome copies (GC); ReninAAV ×1, 1 × 10¹⁰ GC; ReninAAV ×2, 2 × 10¹⁰ GC; ReninAAV ×4, 4 × 10¹⁰ GC; and ReninAAV ×10, 10 × 10¹⁰ GC. **P* < 0.05 and †*P* < 0.01 vs. LacZAAV ×2 (Dunnett's test one-factor/two-factor linear model with interaction). GFR, glomerular filtration rate.

Lisinopril and Empagliflozin Combination Treatment Improves Urinary Markers of Kidney Disease in *db/db* UNx-ReninAAV Mice

Physiological parameters are shown in Table 2 and provided in Supplemental Table S2. Empagliflozin and lisinopril + empagliflozin increased body weight gain accompanied by marked and sustained improvements in hyperglycemia and HbA1c levels in *db/db* UNx-ReninAAV mice (Fig. 2, A–C). Lisinopril was weight neutral and had no effect on glycemic parameters. Terminal plasma urea and cystatin C levels were unaffected in *db/db* UNx-LacZAAV and *db/db* UNx-ReninAAV mice. Plasma urea, but not cystatin C, concentrations were significantly elevated by lisinopril and lisinopril + empagliflozin (Fig. 2, D and E). Urine ACR was significantly elevated in *db/db* UNx-LacZAAV controls (19-fold increase, *P* < 0.001 vs. *db/m* mice). *db/db* UNx-ReninAAV controls exhibited a substantial increase in urine ACR (235-fold vs. *db/m* mice, *P* < 0.001; 12-fold vs. LacZAAV mice, *P* < 0.001), which was significantly reduced by lisinopril and lisinopril + empagliflozin (*P* < 0.001 vs. vehicle control; see Fig. 2F).

Lisinopril and Empagliflozin Combination Treatment Improves Kidney Histopathology in *db/db* UNx-ReninAAV Mice

A deep learning-based method was developed and applied for automated detection of glomeruli and scoring of glomerulosclerosis (Fig. 3A). Although the glomerular population in *db/m* mice was overall normal (>95% with GS0), glomerulosclerosis scores were consistently higher in *db/db* UNx mice (Fig. 3, A–C). Notably, the proportion of mice presenting severe or global glomerulosclerotic lesions (GS3 and GS4) was significantly higher in *db/db* UNx-ReninAAV controls (54 ± 8%) compared with *db/db* UNx-LacZAAV controls (28 ± 5%, *P* < 0.01; Fig. 3D). The glomerulosclerosis index was significantly improved by lisinopril (*P* < 0.05) and lisinopril + empagliflozin (*P* <

0.001; Fig. 3C), largely driven by a reduced proportion of glomeruli with GS3 and GS4 (Fig. 3D and Supplemental Fig. S2). Empagliflozin slightly, but significantly, increased the glomerulosclerosis index and GS3 and GS4 fractions (Fig. 3, C and D). The glomerulosclerosis index and albuminuria were significantly correlated ($r^2 = 0.86$, *P* < 0.001; Supplemental Fig. S3). Cortical collagen type III was significantly elevated in *db/db* UNx-ReninAAV mice but not *db/db* UNx-LacZAAV mice compared with *db/m* mice. Lisinopril + empagliflozin, but not monotherapies, reduced collagen type III expression (*P* < 0.05; Fig. 3, E and F). Kidney KIM-1 staining was almost absent in *db/m* and *db/db* UNx-LacZAAV controls but robustly increased in vehicle-dosed *db/db* UNx-ReninAAV mice. KIM-1 expression was predominantly observed in tubular cells and to a lesser degree in Bowman's capsule (Fig. 3, G and H, and Supplemental Fig. S2). KIM-1 expression in *db/db* UNx-ReninAAV mice was nearly normalized by lisinopril and lisinopril + empagliflozin (both *P* < 0.001; Fig. 3, G and H, and Supplemental Fig. S1). Cortical CD11b-positive immune cell infiltration was pronounced in *db/db* UNx-ReninAAV mice compared with *db/db* UNx-LacZAAV controls (*P* < 0.001). Lisinopril and lisinopril + empagliflozin, but not empagliflozin alone, significantly reduced CD11b levels in *db/db* UNx-ReninAAV mice (Fig. 3, I and J, and Supplemental Fig. S2).

Lisinopril and Empagliflozin Combination Treatment Attenuates Glomerular Hypertrophy in *db/db* UNx-ReninAAV Mice

db/db UNx mice demonstrated kidney hypertrophy, which was unaffected by treatment intervention (Table 1). Glomerular hypertrophy was evident in *db/db* UNx LacZAAV controls and further aggravated in *db/db* UNx-ReninAAV mice (Fig. 4, A–C, and Supplemental Movies S1–S6). UNx and ReninAAV additively stimulated glomerular hypertrophy (Fig. 4B). Lisinopril + empagliflozin significantly reduced total glomerular volume in *db/db* UNx-ReninAAV mice (*P* < 0.05; Fig. 4, B and C). Empagliflozin monotherapy

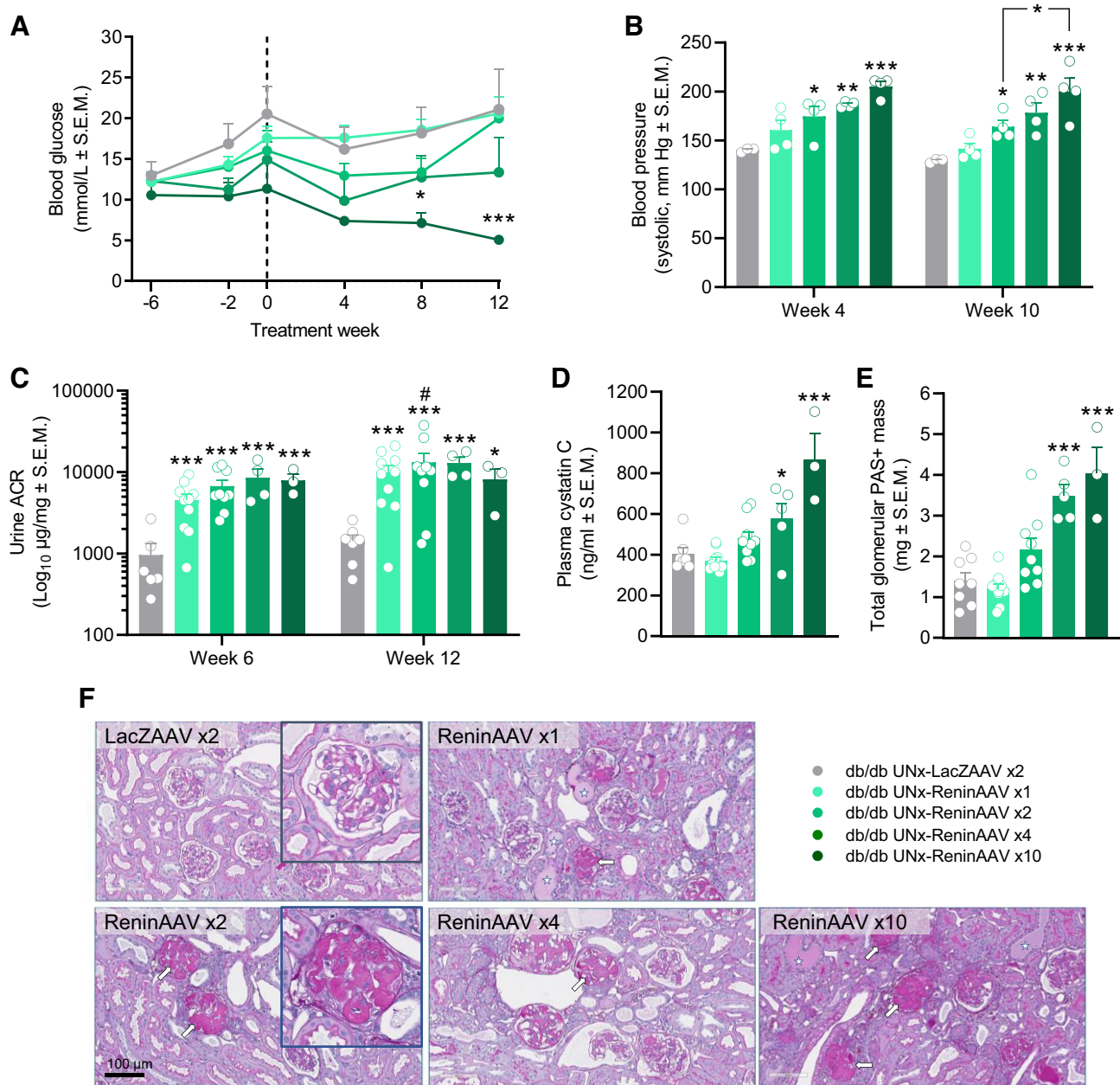


Figure 1. Adeno-associated virus (AAV) delivery of renin promotes hypertension-accelerated kidney disease in uninephrectomized (UNx) diabetic *db/db* mice. ReninAAV dose-dependent effects on physiological parameters and glomerulosclerosis in *db/db* UNx mice are shown. AAV was administered in week -5 , and UNx was performed in week -4 (LacZAAV: $n=7$, ReninAAV $\times 1$: $n=10$, ReninAAV $\times 2$: $n=9$, ReninAAV $\times 4$: $n=4$, and ReninAAV $\times 10$: $n=3$). **A:** fed blood glucose levels. **B:** blood pressure. **C:** urine albumin-to-creatinine ratio (ACR; log transformation). **D:** plasma levels of cystatin C. **E:** artificial intelligence-assisted identification and quantification of glomerular periodic acid-Schiff (PAS) staining. **F:** representative photomicrographs of glomerulosclerosis pathology in *db/db* UNx ReninAAV mice. Arrows highlight global sclerotic glomeruli; stars indicate intratubular casts. See the insets for representative glomerulus morphology. LacZAAV $\times 2$, 2×10^{10} genome copies (GC); ReninAAV $\times 1$, 1×10^{10} GC; ReninAAV $\times 2$, 2×10^{10} GC; ReninAAV $\times 4$, 4×10^{10} GC; ReninAAV $\times 10$, 10×10^{10} GC. * $P < 0.05$, ** $P < 0.01$, and *** $P < 0.001$ vs. *db/db* UNx-LacZAAV $\times 2$ mice; # $P < 0.05$ vs. the corresponding level in treatment week 6 (Dunnett's test one-factor/two-factor linear model with interaction).

slightly increased glomerular volume ($P < 0.05$; Fig. 4, A–C, and Supplemental Movies S1–S6). No significant differences in the total number of glomeruli per kidney were observed between groups (Fig. 4D). Cardiac hypertrophy was most pronounced in ReninAAV groups (Tables 1 and 2), slightly accentuated by empagliflozin, and partially reversed by lisinopril and lisinopril + empagliflozin (Table 2).

DISCUSSION

Persistent hypertension established by ReninAAV promoted further progression of kidney disease in diabetic *db/db* UNx mice. Kidney injury was attenuated in *db/db* UNx-ReninAAV mice following long-term combination treatment with lisinopril and empagliflozin. The clear pathological hallmarks of DKD and therapeutic response to the standard

Table 2. Treatment intervention study

	db/m	db/db UNx- LacZAAV Vehicle	db/db UNx- ReninAAV Vehicle	db/db UNx- ReninAAV Lisinopril	db/db UNx- ReninAAV Empagliflozin	db/db UNx- ReninAAV Lisinopril + Empagliflozin
Survival rate, <i>n</i>	8/8	15/15	17/18	17/18	17/18	17/18
Body weight at randomization (<i>day</i> -2), g	22.0 ± 0.2 ^c	45.2 ± 0.7	44.8 ± 1.0	44.6 ± 1.2	43.9 ± 1.1	44.8 ± 1.1
Fed blood glucose at randomization (<i>day</i> -2), mmol/L	ND	18.9 ± 1.2	18.2 ± 2.0	17.1 ± 1.6	16.4 ± 1.5	17.5 ± 1.4
Body weight (<i>week</i> 12), g	23.8 ± 0.4 ^c	42.7 ± 1.9	44.7 ± 2.1	43.5 ± 1.8	50.5 ± 1.6 ^a	50.7 ± 1.8 ^c
Fed blood glucose (<i>week</i> 12), mmol/L	6.4 ± 0.1 ^c	21.6 ± 1.1	18.0 ± 1.9	21.0 ± 2.0	12.3 ± 1.5 ^a	13.1 ± 1.0
Kidney weight (<i>week</i> 12), mg	158 ± 4.7 ^c	311 ± 11.1	323 ± 10.0	306 ± 10.7	344 ± 9.0	332 ± 9.6
Relative kidney weight (<i>week</i> 12), mg/g body wt	6.6 ± 0.2	7.5 ± 0.4	7.5 ± 0.5	7.2 ± 0.3	6.9 ± 0.3	6.6 ± 0.2
Heart weight (<i>week</i> 12), mg	126 ± 2.7 ^c	147 ± 3.7 ^c	202 ± 6.3	179 ± 5.9 ^b	229 ± 6.1 ^b	182 ± 5.0 ^{a,f}
Relative heart weight (<i>week</i> 12), mg/g body wt	5.3 ± 0.1 ^a	3.5 ± 0.1 ^c	4.7 ± 0.2	4.1 ± 0.1	4.6 ± 0.1	3.6 ± 0.1 ^{c,d,f}

All data are presented as means ± SE; *n*, number of mice. Physiological data in diabetic *db/db* uninephrectomized (UNx)-ReninAAV mice administered lisinopril, empagliflozin, or combination for 12 wk are shown. Adeno-associated virus (AAV) LacZ or renin construct (2×10^{10} genome copies) was intravenously administered in *study week* -5 (7 wk of age), and UNx was performed in female *db/db* mice in *study week* -4. *db/db* UNx-ReninAAV mice received vehicle (PO, QD), lisinopril (40 mg/kg, PO, QD), empagliflozin (20 mg/kg, PO, QD), or lisinopril + empagliflozin combination treatment (40 mg/kg + 20 mg/kg, PO, QD) for 12 wk. Mice were euthanized after 17 wk of single AAV exposure, corresponding to treatment *week* 12. Nondiabetic female *db/m* mice served as untreated normal controls; vehicle-dosed female *db/db* UNx-LacZAAV served as diabetic UNx controls. Data are only shown from mice that completed the entire study. ^a*P* < 0.05, ^b*P* < 0.01, and ^c*P* < 0.001 vs. *db/db* UNx-ReninAAV vehicle; ^d*P* < 0.01 and ^e*P* < 0.001 vs. lisinopril monotherapy; ^f*P* < 0.001 vs. empagliflozin monotherapy (Dunnett's test one-factor/two-factor linear model with interaction). ND, not determined.

of medical care highlight the suitability of the *db/db* UNx-ReninAAV mouse model for characterizing novel drug therapies for DKD in the setting of T2D and hypertension.

Chronic hypertension induced by overexpression of renin, independent from intrinsic homeostatic feedback mechanisms, represents emerging models of DKD (29–31). A promising model of progressive DKD has recently been established by AAV delivery of renin superimposed on baseline kidney disease in diabetic *db/db* UNx mice (12). We therefore evaluated the *db/db* UNx-ReninAAV mouse model of DKD in further detail. ReninAAV dose dependently elevated systolic arterial blood pressure in *db/db* UNx mice, which persisted for at least 17 wk. The degree of hypertension attained by a single injection of ReninAAV was similar to previous studies and is consistent with corresponding ReninAAV dose-dependent increases in plasma renin levels and renin activity in *db/db* UNx-ReninAAV mice (12, 17). The majority of AAV integrates in the liver, including the AAV serotype used in the current study (32). In combination with the use of renin expression driven by a liver-specific promoter, renin overexpression occurs specifically at the level of the liver, whereupon the gene product is released into the circulation (12, 17). *db/db* UNx-ReninAAV mice show compensatory downregulation of kidney renin expression (unpublished observations), reflecting chronic systemic renin overactivity in the model. It should, therefore, be considered that kidney pathology in the model is likely independent of intrarenal renin expression.

Although all ReninAAV doses were equally effective in increasing ACR and dose dependently worsened glomerulosclerosis, the use of high ReninAAV titers ($\geq 4 \times 10^{10}$ GC) was precluded due to reduced survival rate. GFR was similar in ReninAAV- and LacZAAV-injected *db/db* UNx mice, as measured by FITC-sinistrin clearance. Correspondingly, ReninAAV doses up to 2×10^{10} GC did not influence terminal plasma cystatin C levels, a marker of GFR (33). Taken together, this indicates sustained GFR in *db/db* UNx-ReninAAV mice, and GFR was therefore not evaluated in the treatment intervention study. Reduced GFR has been previously reported 8 wk after

ReninAAV injection, using a lower ReninAAV dose in older *db/db* UNx mice (5×10^9 GC, dosing at 12 wk of age) (12). It should be noted that the study by Harlan et al. (12) only reported GFR data for a minor subpopulation (*n* = 5) of mice with signs of significant renal impairment (doubling of creatinine). In addition, differences in ReninAAV titer as well as timing of administration and GFR assessment could potentially explain the discrepancy between the present study and the study by Harlan et al. (12). Compared with untreated normoglycemic *db/m* mice, *db/db* UNx-ReninAAV mice developed extreme albuminuria, a key diagnostic criteria in human DKD (34, 35). In accordance, consistent pathological features in *db/db* UNx-ReninAAV mice included severe glomerulosclerosis and tubular injury, glomerular hypertrophy, and monocyte infiltration. Increased glomerular volume was also observed in *db/db* UNx-LacZAAV mice. This is consistent with a recent whole kidney 3D imaging study demonstrating glomerular hypertrophy in *db/db* mice and is augmented by UNx (20). Consistent with the absence of GFR decline, *db/db* UNx-ReninAAV mice did not develop tubulointerstitial fibrosis, which is inversely correlated to kidney function (36). However, *db/db* UNx-ReninAAV, but not LacZAAV mice demonstrated robust upregulation of KIM-1 expression, a histological marker of proximal tubular epithelial cell damage (37). In summary, kidney pathology in *db/db* UNx-ReninAAV mice mirrors human progressive DKD anteceding decline in renal function and tubulointerstitial fibrosis.

The standard of care for the management of hypertension (lisinopril) and hyperglycemia (empagliflozin) attenuated kidney disease in the model. Consistent with intrarenal RAAS overactivity playing a cardinal role in the pathogenesis and management of DKD (38), 12 wk of lisinopril monotherapy robustly improved extreme albuminuria in *db/db* UNx-ReninAAV mice. This effect was accompanied by slightly elevated plasma urea levels. It should be noted that circulating urea levels are a poor indicator of GFR as the liver synthesis rate depends on several nonrenal factors, including urea cycle enzyme activity. Improved albuminuria may

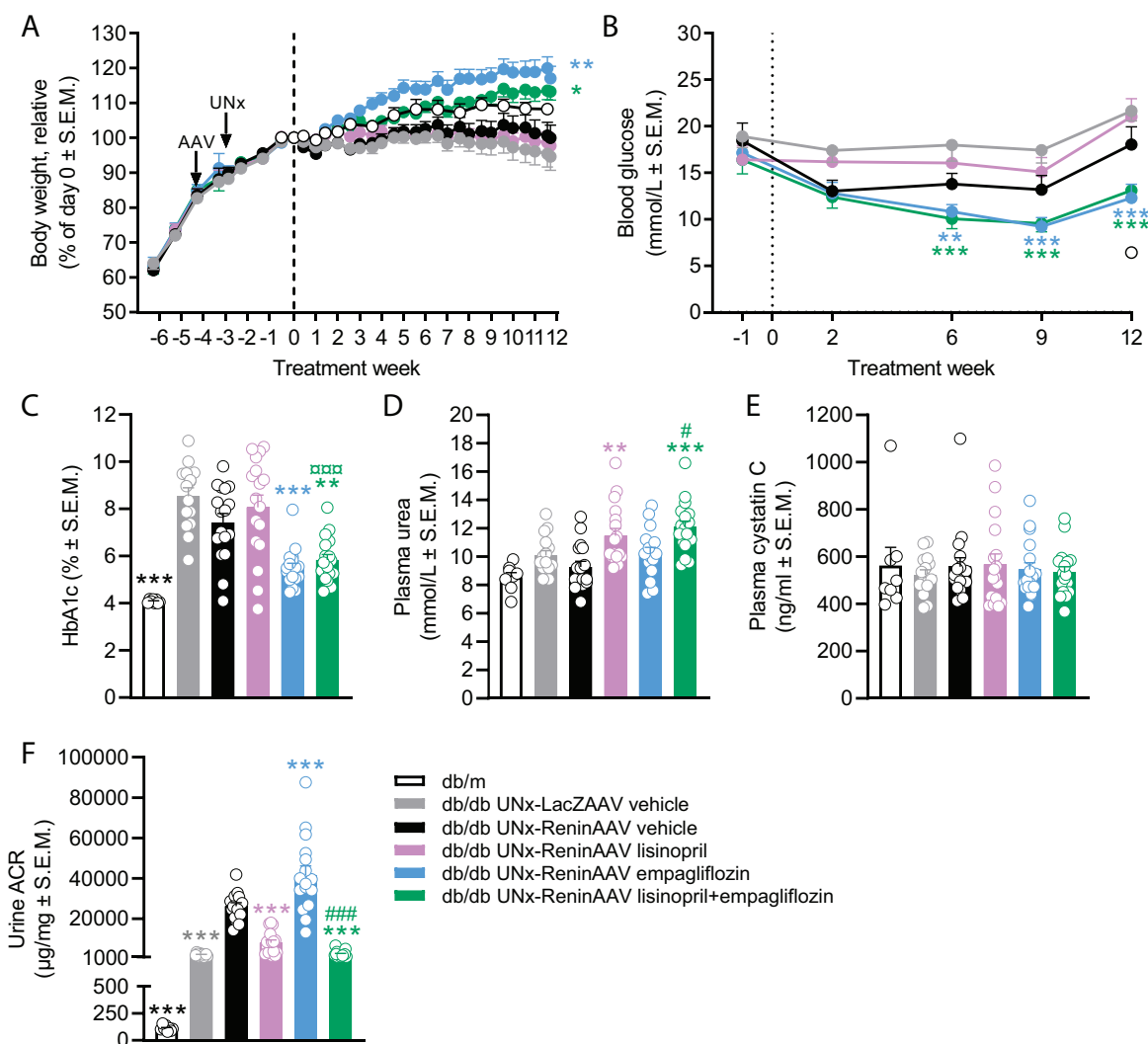


Figure 2. Lisinopril and empagliflozin combination treatment improves plasma and urine markers of kidney disease in *db/db* uninephrectomized (UNx)-ReninAAV mice. Shown is the characterization of lisinopril (40 mg/kg, PO, QD, $n=17$), empagliflozin (20 mg/kg, PO, QD, $n=17$), and combination treatment (40 + 20 mg/kg, PO, QD, $n=17$) for 12 wk in *db/db* UNx-ReninAAV mice (AAV-renin dose, 2×10^{10} genome copies). Untreated *db/m* ($n=8$), vehicle-dosed *db/db* UNx-LacZAAV ($n=15$), and vehicle-dosed *db/db* UNx-ReninAAV ($n=17$) mice served as controls. **A:** body weight. **B:** fed blood glucose levels. The open circle indicates blood glucose levels in *db/m* control mice (week 12). **C:** HbA1c levels. **D:** plasma urea concentrations. **E:** plasma cystatin C levels. **F:** urine albumin-to-creatinine ratio (ACR). AAV, adeno-associated virus. * $P < 0.05$, ** $P < 0.01$, and *** $P < 0.001$ vs. vehicle-dosed *db/db* UNx-ReninAAV mice; °°° $P < 0.001$ vs. lisinopril monotherapy; # $P < 0.05$ vs. empagliflozin monotherapy (Dunnett's test one-factor/two-factor linear model with interaction). AAV, adeno-associated virus.

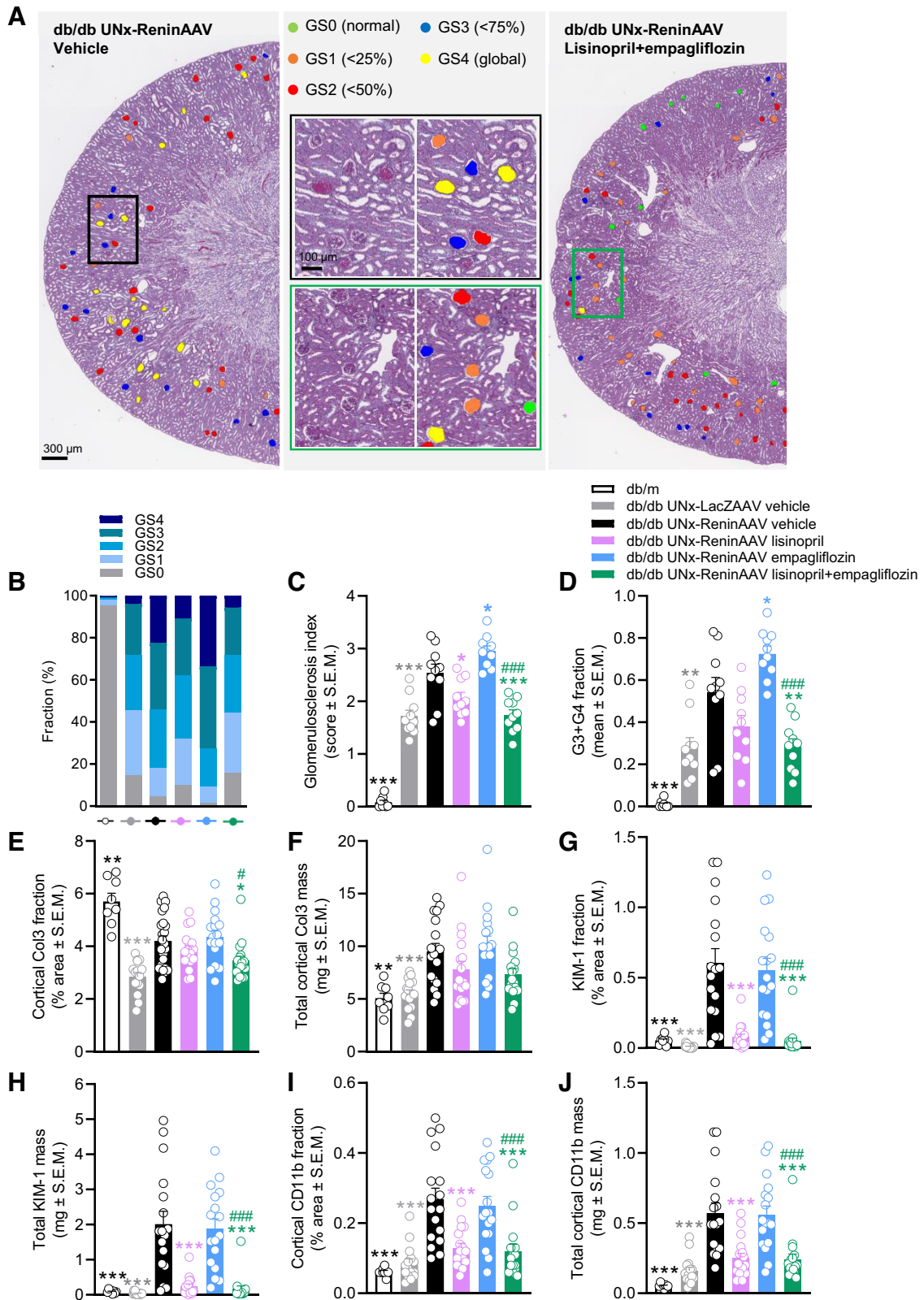
primarily reflect lowered intraglomerular pressure and correlates with reduced inflammation, endothelial dysfunction, and fibrosis, resulting in less long-term kidney injury (39, 40). The improved glomerular function following lisinopril treatment was supported by reduced glomerulosclerosis. Reduced infiltration of CD11-positive monocytes following lisinopril treatment was paralleled by marked suppression of KIM-1 expression. Renal KIM-1 overexpression has been linked to macrophage-driven tubule interstitial inflammation (41). Notably, the addition of empagliflozin to lisinopril treatment resulted in further robust renal improvements in *db/db* UNx-ReninAAV mice. Accordingly, only combined lisinopril and empagliflozin treatment significantly reduced glomeruli populations with severe or global glomerulosclerotic lesions. In addition, only combination therapy significantly improved cortical collagen type III deposition and whole kidney

glomerular hypertrophy, further arguing for contributory therapeutic effects of SGLT2 inhibition. Compared with lisinopril monotherapy, lisinopril and empagliflozin cotreatment resulted in slightly more pronounced improvement in key histological end points in *db/db* UNx-ReninAAV mice. It is therefore conceivable that histological outcomes following drug combination treatment were mostly attributed to systemic and renal hemodynamic effects of lisinopril.

Our study corroborates and extends findings of robust nephroprotective effects of lisinopril in combination with antidiabetic treatment (rosiglitazone) in *db/db* UNx-ReninAAV mice (11, 12). Enhanced therapeutic effects of combined lisinopril and empagliflozin administration may relate to their different modes of action. The principal nephroprotective mechanism of RAAS inhibitors is a reduction of intraglomerular pressure by limiting angiotensin II-induced vasoconstriction of the

efferent arteriole (42). In addition, nephroprotective effects of RAAS blockade have been attributed to direct action on nephron components, including the podocyte (43). Although reduced glucotoxicity and metabolic stimulation of tissue

oxygen delivery may, at least in part, underlie the cardiorenal effects of SGLT2 inhibitors (44), this drug class may also have direct nephroprotective properties independent of glycemic effects. This notion is strengthened by clinical trials



demonstrating comparable beneficial effects of SGLT2 inhibitors on renal end points in both diabetic and nondiabetic patients with CKD (8–10). By blocking proximal tubular glucose and sodium reabsorption, SGLT2 inhibitors increase sodium delivery to the juxtaglomerular apparatus, thereby activating macular densa cells, which is a key mechanism to restore tubuloglomerular autoregulation, leading to afferent arteriolar constriction, reduced intraglomerular hypertension, and a decrease in hyperfiltration (45–47).

Empagliflozin monotherapy exacerbated albuminuria, glomerulosclerosis, glomerular hypertrophy, and cardiac hypertrophy, which were completely prevented by lisinopril coadministration. This suggests further RAAS stimulation following empagliflozin administration in *db/db* UNx-ReninAAV mice. Empagliflozin administration has been reported to stimulate plasma and cortical renin activity in both *db/m* and diabetic *db/db* mice (48). Correspondingly, increased plasma renin activity as well as elevated plasma levels of angiotensin II and aldosterone have been observed in patients with diabetes following short-term empagliflozin and dapagliflozin treatment (49, 50), likely attributed to intravascular volume depletion, a well-known effect of SGLT2 inhibitors (45, 49, 51). Although cardiac hypertrophy in empagliflozin-treated *db/db* UNx-ReninAAV mice may indirectly suggest further stimulated RAAS activity and hypertension, this must be specifically addressed by blood pressure analysis. Although chronic hypertension was confirmed in the ReninAAV dose-finding study, tail-cuff plethysmography was not applied in the treatment study as the procedure may cause handling and restraint stress, which could negatively affect blood pressure and therefore potentially influence treatment outcomes in the model.

Current clinical trials on SGLT2 inhibitors in diabetic and nondiabetic patients with CKD have been performed with background antihypertensive therapy, typically RAAS blockade (7–10). Although effects of SGLT2 monotherapy remains to be established in patients with DKD, preclinical studies have yielded inconsistent results on SGLT2 inhibitor treatment in DKD/CKD models. Accordingly, empagliflozin and dapagliflozin have demonstrated no effect or attenuate renal end points in normotensive diabetes models with features of mild-moderate kidney pathology, including *db/db* mice (48, 52–56). Empagliflozin has been demonstrated to prevent the development of glomerular and tubulointerstitial fibrosis, but not GFR loss, following angiotensin II infusion or 5/6 nephrectomy in nondiabetic rodents (56–58). Although dapagliflozin showed no glomeruloprotective effect when administered 1 wk after 5/6 nephrectomy (59), canagliflozin treatment starting 1 wk after angiotensin II infusion has

been reported to improve GFR and improve glomerulosclerosis in normoglycemic mice (60). Collectively, it may be speculated that the timing of SGLT2 inhibitor administration is critical for observing therapeutic effects in DKD/CKD models with established progressive kidney disease.

In contrast to lisinopril, empagliflozin increased body weight concurrent with improved hyperglycemia. Similar to *db/db* UNx-ReninAAV mice, long-term empagliflozin treatment has been previously reported to increase body weight and insulin levels, but not food intake, in *db/db* mice (48, 61). Considering that body weight in *db/db* mice gradually reaches a plateau and may eventually decline as a consequence of long-standing deteriorating hyperglycemia and insufficient insulin secretion (62), it is conceivable that sustained body weight gain in empagliflozin-treated *db/db* UNx-ReninAAV mice is a consequence of improved glucose handling.

Limitations of the study should be considered. Because blood pressure was not monitored in the treatment study, it remains to be determined to what degree the slightly more robust effects of lisinopril and empagliflozin combination treatment on kidney histological endpoints may be explained by contributory mechanisms unrelated to blood pressure regulation. Although our study provides pharmacological validation of *db/db* UNx-ReninAAV mice as a preclinical model of advanced DKD, using lisinopril alone and in combination with empagliflozin, future studies in *db/db* UNx-ReninAAV mice must aim to broader define treatment responses in the model by profiling drug classes targeting other pathophysiological mechanisms in DKD. Also, the present study was limited to define kidney disease for up to 17 wk after ReninAAV administration in female *db/db* UNx mice. Considering the clear indication of extreme albuminuria and advanced glomerulosclerosis, we cannot exclude worsening kidney function beyond this observation period. Although it would be relevant also to characterize DKD progression and standard of care in older *db/db* UNx-ReninAAV mice, this may be incompatible with progressively deteriorating hyperglycemia and resulting reduced longevity in *db/db* mice.

In conclusion, the present study substantiates hypertension and diabetes as essential components in the progression of DKD and further supports *db/db* UNx-ReninAAV mice as a clinical translational model of advanced DKD. The therapeutic effects of the standard of care to control hypertension and hyperglycemia provides a proof of concept for testing novel drug therapies in the *db/db* UNx-ReninAAV mouse model of DKD.

Figure 3. Lisinopril and empagliflozin combination treatment improves glomerulosclerosis in *db/db* uninephrectomized (UNx)-ReninAAV mice. **A:** automated detection of periodic acid-Schiff-positive glomeruli and scoring of glomerulosclerosis. A scoring-based color code was used to visualize sclerosis severity (GS0–GS4) in affected glomeruli. Representative images are from vehicle-dosed and lisinopril + empagliflozin-treated *db/db* UNx-ReninAAV mice, respectively. **Insets:** further magnification ($\times 20$) of the selected areas. **B:** distribution of glomerulosclerosis scores in *db/db* mice ($n=8$), vehicle-dosed *db/db* UNx-LacZAAV control mice ($n=10$), and *db/db* UNx-ReninAAV mice that received vehicle, lisinopril (40 mg/kg, PO, QD, $n=10$), empagliflozin (20 mg/kg, PO, QD, $n=10$), or lisinopril + empagliflozin (40 + 20 mg/kg, PO, QD, $n=10$). **C:** group-wise distribution (fraction %) of glomerulosclerosis scores. **D:** glomerulosclerosis index. **E:** fraction of glomeruli with severe or global glomerulosclerosis (GS3 + GS4). **F:** percent area of cortical collagen type III (Col3). **G:** total cortical Col3 mass. **H:** percent area of kidney injury molecule-1 (KIM-1). **I:** total KIM-1 mass. **J:** percent area of cortical CD11b mass. * $P < 0.05$, ** $P < 0.01$, and *** $P < 0.001$ vs. *db/db* UNx-ReninAAV control mice; # $P < 0.05$ and ### $P < 0.001$ vs. empagliflozin monotherapy (Dunnett's test one-factor linear model with interaction). AAV, adeno-associated virus; GS, glomerulosclerosis scores.

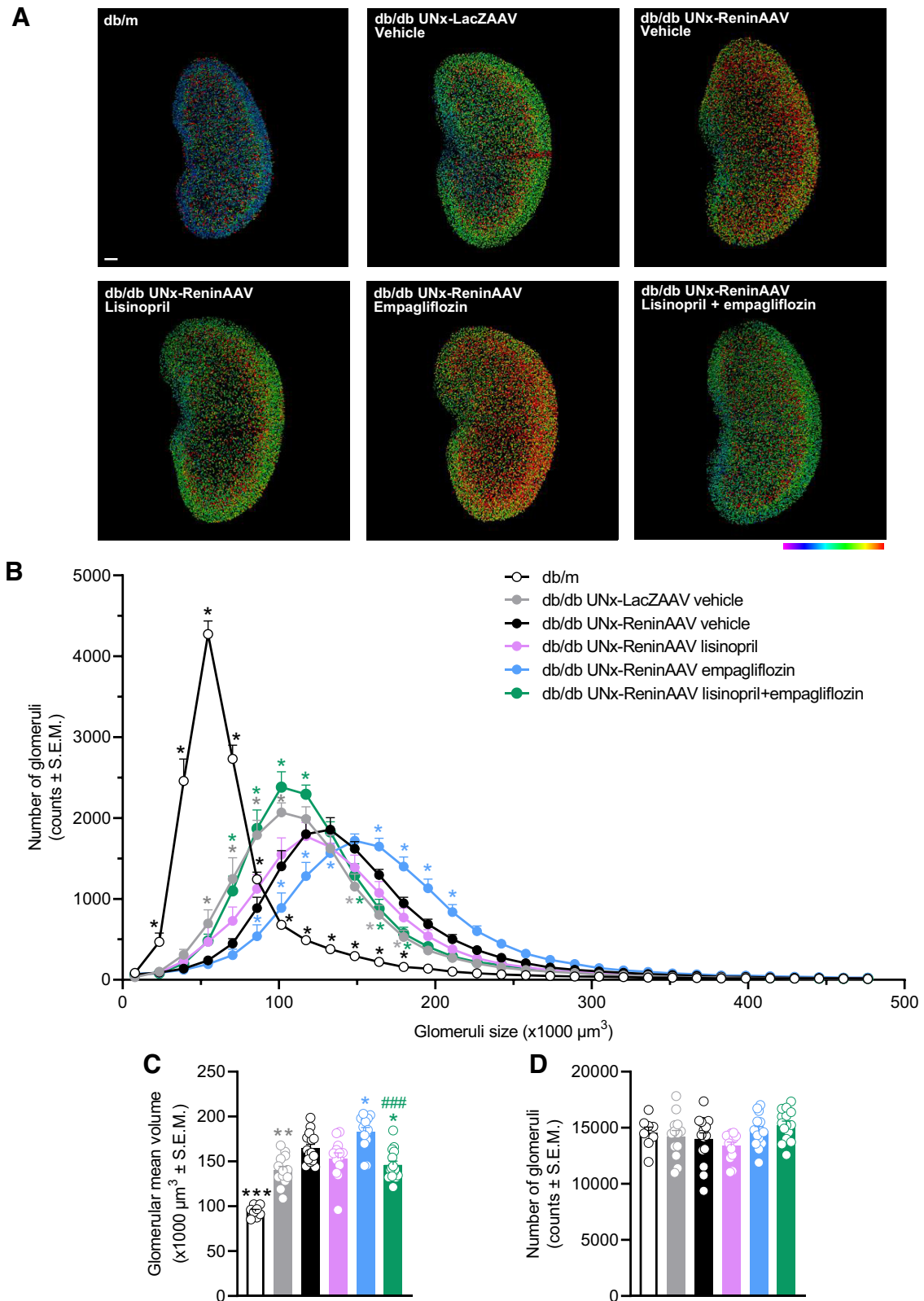


Figure 4. Lisinopril and empagliflozin combination treatment attenuates glomerular hypertrophy in *db/db* uninephrectomized (UNx)-ReninAAV mice. **A:** 3D reconstruction of representative kidneys from *db/m* ($n=8$), *db/db* UNx-LacZAAV ($n=13$), and *db/db* UNx-ReninAAV mice that received vehicle ($n=13$), lisinopril (40 mg/kg, PO, QD, $n=15$), empagliflozin (20 mg/kg, PO, QD, $n=13$), or lisinopril + empagliflozin (40 + 20 mg/kg, PO, QD, $n=15$). Scale bar = 700 μm . A volume-based color code was used to visualize the volume of each individual glomerulus, ranging from 20 (blue) to $250 \times 1,000 \mu\text{m}^3$ (red). **B:** volume distribution frequency plot. **C:** glomerular mean volume. **D:** whole kidney glomerular number. * $P < 0.05$, ** $P < 0.01$, and *** $P < 0.001$ vs. vehicle-dosed *db/db* UNx-ReninAAV mice (Dunnett's test one-factor/two-factor linear model with interaction). AAV, adeno-associated virus.

SUPPLEMENTAL DATA

All Supplemental Material: <https://doi.org/10.6084/m9.figshare.14431229.v1>.

ACKNOWLEDGMENTS

The authors acknowledge skilled technical assistance by Malene A. Christensen and Frederikke E. Sembach.

GRANTS

Authors received no funding for the research of this article.

DISCLOSURES

No conflicts of interest, financial or otherwise, are declared by the authors.

AUTHOR CONTRIBUTIONS

M.V.Ø., J.J., N.V., and L.N.F. conceived and designed research; T.S., I.R., M.C., C.G.S., U.R., and J.L.S. performed experiments; M.V.Ø., T.S., M.C., C.G.S., U.R., J.L.S., I.R., H.H.H., J.J., N.V., and L.N.F. analyzed data; M.V.Ø., T.S., M.C., C.G.S., U.R., J.L.S., H.H.H., J.J., N.V., and L.N.F. interpreted results of experiments; T.S., C.G.S., U.R., and H.H.H. prepared figures; M.V.Ø., T.S., C.G.S., J.L.S., I.R., H.H.H., and J.J. drafted manuscript; M.V.Ø., T.S., C.G.S., U.R., J.L.S., I.R., H.H.H., J.J., and L.N.F. edited and revised manuscript; M.V.Ø., T.S., M.C., C.G.S., U.R., J.L.S., I.R., H.H.H., J.J., N.V., and L.N.F. approved final version of manuscript.

REFERENCES

- Kainz A, Hronsky M, Stel VS, Jager KJ, Geroldinger A, Dunkler D, Heinze G, Tripepi G, Oberbauer R. Prediction of prevalence of chronic kidney disease in diabetic patients in countries of the European Union up to 2025. *Nephrol Dial Transplant* 30, Suppl 4: iv113–iv118, 2015. doi:10.1093/ndt/gfv073.
- Wu B, Bell K, Stanford A, Kern DM, Tunceli O, Vupputuri S, Kalsekar I, Willey V. Understanding CKD among patients with T2DM: prevalence, temporal trends, and treatment patterns—NHANES 2007–2012. *BMJ Open Diabetes Res Care* 4: e000154, 2016. doi:10.1136/bmjdr-2015-000154.
- Thomas MC, Brownlee M, Susztak K, Sharma K, Jandeleit-Dahm KAM, Zoungas S, Rossing P, Groop P-H, Cooper ME. Diabetic kidney disease. *Nat Rev Dis Primers* 1: 15018, 2015. doi:10.1038/nrdp.2015.18.
- Brenner BM, Cooper ME, De Zeeuw D, Keane WF, Mitch WE, Parving HH, Remuzzi G, Snapinn SM, Zhang Z, Shahinfar S; REENAL Study Investigators. Effects of losartan on renal and cardiovascular outcomes in patients with type 2 diabetes and nephropathy. *N Engl J Med* 345: 861–869, 2001. doi:10.1056/NEJMoa011161.
- Lewis EJ, Hunsicker LG, Bain RP, Rohde RD. The effect of angiotensin-converting-enzyme inhibition on diabetic nephropathy. The Collaborative Study Group. *N Engl J Med* 329: 1456–1462, 1993. doi:10.1056/NEJM19931113292004.
- Strippoli GFM, Craig M, Deeks JJ, Schena FP, Craig JC. Effects of angiotensin converting enzyme inhibitors and angiotensin II receptor antagonists on mortality and renal outcomes in diabetic nephropathy: systematic review. *BMJ* 329: 828, 2004. doi:10.1136/bmj.38237.585000.7C.
- Heerspink HJL, Stefánsson BV, Correa-Rotter R, Chertow GM, Greene T, Hou F-F, Mann JFE, McMurray JVV, Lindberg M, Rossing P, Sjöström CD, Toto RD, Langkilde A-M, Wheeler DC; DAPA-CKD Trial Committees and Investigators. Dapagliflozin in patients with chronic kidney disease. *N Engl J Med* 383: 1436–1446, 2020. doi:10.1056/NEJMoa2024816.
- Cherney DZI, Dekkers CCJ, Barbour SJ, Cattran D, Abdul Gafor AH, Greasley PJ, Laverman GD, Lim SK, Di Tanna GL, Reich HN, Vervloet MG, Wong MG, Gansevoort RT, Heerspink HJL. Effects of the SGLT2 inhibitor dapagliflozin on proteinuria in non-diabetic patients with chronic kidney disease (DIAMOND): a randomised, double-blind, crossover trial. *Lancet Diabetes Endocrinol* 8: 582–593, 2020. doi:10.1016/S2213-8587(20)30162-5.
- Perkovic V, de Zeeuw D, Mahaffey KW, Fulcher G, Erond N, Shaw W, Barrett TD, Weidner-Wells M, Deng H, Matthews DR, Neal B. Canagliflozin and renal outcomes in type 2 diabetes: results from the CANVAS Program randomised clinical trials. *Lancet Diabetes Endocrinol* 6: 691–704, 2018. doi:10.1016/S2213-8587(18)30141-4.
- Wanner C, Inzucchi SE, Lachin JM, Fitchett D, von Eynatten M, Mattheus M, Johansen OE, Woerle HJ, Broedl UC, Zinman B; EMPA-REG OUTCOME Investigators. Empagliflozin and progression of kidney disease in type 2 diabetes. *N Engl J Med* 375: 323–334, 2016. doi:10.1056/NEJMoa1515920.
- Harlan SM, Heinz-Taheny KM, Overstreet JM, Breyer MD, Harris RC, Heuer JG. Pathological and transcriptome changes in the ReninAAV *db/db* uNx model of advanced diabetic kidney disease exhibit features of human disease. *Toxicol Pathol* 46: 991–998, 2018. doi:10.1177/0192623318804986.
- Harlan SM, Heinz-Taheny KM, Sullivan JM, Wei T, Baker HE, Jaqua DL, Qi Z, Cramer MS, Shiyanova TL, Breyer MD, Heuer JG. Progressive renal disease established by renin-coding adeno-associated virus-driven hypertension in diverse diabetic models. *J Am Soc Nephrol* 29: 477–491, 2018. doi:10.1681/ASN.2017040385.
- Ninomiya H, Inomata T, Ogihara K. Obstructive uropathy and hydronephrosis in male KK-Ay mice: a report of cases. *J Vet Med Sci* 61: 53–57, 1999. doi:10.1292/jvms.61.53.
- Sembach FE, Fink LN, Johansen T, Boland BB, Secher T, Thrane ST, Nielsen JC, Fosgerau K, Vrang N, Jelsing J, Pedersen TX, Østergaard MV. Impact of sex on diabetic nephropathy and the renal transcriptome in UNx *db/db* C57BLKS mice. *Physiol Rep* 7: e14333, 2019. doi:10.14814/phy2.14333.
- Springer DA, Allen M, Hoffman V, Brinster L, Starost MF, Bryant M, Eckhaus M. Investigation and identification of etiologies involved in the development of acquired hydronephrosis in aged laboratory mice with the use of high-frequency ultrasound imaging. *Pathobiol Aging Age-related Dis* 4: 24932, 2014. doi:10.3402/pba.v4.24932.
- Caron KMI, James LR, Kim HS, Morham SG, Sequeira Lopez MLS, Gomez RA, Reudelhuber TL, Smithies O. A genetically clamped renin transgene for the induction of hypertension. *Proc Natl Acad Sci USA* 99: 8248–8252, 2002. doi:10.1073/pnas.112221999.
- Harlan SM, Ostroski RA, Coskun T, Yantis LD, Breyer MD, Heuer JG. Viral transduction of renin rapidly establishes persistent hypertension in diverse murine strains. *Am J Physiol Regul Integr Comp Physiol* 309: R467–R474, 2015. doi:10.1152/ajpregu.00106.2015.
- Sembach FE, Østergaard MV, Vrang N, Feldt-Rasmussen B, Fosgerau K, Jelsing J, Fink LN. Rodent models of diabetic kidney disease: human translatability and preclinical validity. *Drug Discov Today* 26: 200–217, 2021. doi:10.1016/j.drudis.2020.05.004.
- Schreiber A, Shulhevich Y, Geraci S, Hesser J, Stsepankou D, Neudecker S, Koenig S, Heinrich R, Hoecklin F, Pill J, Friedemann J, Schweda F, Gretz N, Schock-Kusch D. Transcutaneous measurement of renal function in conscious mice. *Am J Physiol Renal Physiol* 303: F783–F788, 2012. doi:10.1152/ajprenal.00279.2012.
- Østergaard MV, Sembach FE, Skytte JL, Roostalu U, Secher T, Overgaard A, Fink LN, Vrang N, Jelsing J, Hecksher-Sørensen J. Automated image analyses of glomerular hypertrophy in a mouse model of diabetic nephropathy. *Kidney360* 1: 469–479, 2020. doi:10.34067/KID.0001272019.
- Østergaard MV, Pinto V, Stevenson K, Worm J, Fink LN, Coward RJM. DBA2J *db/db* mice are susceptible to early albuminuria and glomerulosclerosis that correlate with systemic insulin resistance. *Am J Physiol Renal Physiol* 312: F312–F321, 2017. doi:10.1152/ajprenal.00451.2016.
- Saito T, Sumithran E, Glasgow EF, Atkins RC. The enhancement of aminonucleoside nephrosis by the co-administration of protamine. *Kidney Int* 32: 691–699, 1987. doi:10.1038/ki.1987.262.
- Ronneberger O, Fischer P, Brox T. Convolutional networks for biomedical image segmentation in International Conference on Medical Image Computing and Computer-Assisted Intervention—MICCAI 2015. *MICCAI 2015. Lecture Notes in Computer Science*, edited by

- Navab N, Hornegger J, Wells W, Frangi A. Cham: Springer, 2015, vol. 9351, p. 234–241. doi:10.1007/978-3-319-24574-4_28.
24. Szegedy C, Vanhoucke V, Ioffe S, Shlens J, Wojna Z. *Rethinking the Inception Architecture for Computer Vision*. Las Vegas, NV: 2016 IEEE Conference on Computer Vision and Pattern Recognition, 2016. doi: 10.1109/CVPR.2016.308.
 25. Chollet F, et al. Keras (Online), 2015. <https://github.com/keras-team/keras>.
 26. Kingma D, Adam BJ. *Adam: a Method for Stochastic Optimization*. San Diego, CA: 3rd International Conference for Learning Representations, 2015. <http://arxiv.org/abs/1412.6980>.
 27. Maric C, Sandberg K, Hinojosa-Laborde C. Glomerulosclerosis and tubulointerstitial fibrosis are attenuated with 17 β -estradiol in the aging Dahl salt sensitive rat. *J Am Soc Nephrol* 15: 1546–1556, 2004. doi:10.1097/01.ASN.0000128219.65330.EA.
 28. Robertson RT, Levine ST, Haynes SM, Gutierrez P, Baratta JL, Tan Z, Longmuir KJ. Use of labeled tomato lectin for imaging vasculature structures. *Histochem Cell Biol* 143: 225–234, 2015. doi:10.1007/s00418-014-1301-3.
 29. Cairns C, Conway B. Modeling human diabetic kidney disease by combining hyperglycemia and hypertension in a transgenic rodent model. In: *Methods in Molecular Biology*, edited by Gnudi L, Long D. New York: Humana Press Inc., p. 41–52, 2020. doi:10.1007/978-1-4939-9841-8_4.
 30. Fletcher SJ, Kalupahana NS, Soltani-Bejnood M, Kim JH, Saxton AM, Wasserman DH, De Taeye B, Voy BH, Quignard-Boulangé A, Moustaid-Moussa N. Transgenic mice overexpressing renin exhibit glucose intolerance and diet-genotype interactions. *Front Endocrinol (Lausanne)* 3: 166, 2013. doi:10.3389/fendo.2012.00166.
 31. He X, Zhang T, Tolosa M, Goru SK, Chen X, Misra PS, Robinson LA, Yuen DA. A new, easily generated mouse model of diabetic kidney fibrosis. *Sci Rep* 9: 12549, 2019. doi:10.1038/s41598-019-49012-4.
 32. Cotugno G, Annunziata P, Barone MV, Karali M, Banfi S, Auricchio A. Impact of age at administration, lysosomal storage, and transgene regulatory elements on AAV2/8-mediated rat liver transduction. *PLoS One* 7: e33286, 2012. doi:10.1371/journal.pone.0033286.
 33. Tidman M, Sjöström P, Jones I. A comparison of GFR estimating formulae based upon s-cystatin C and s-creatinine and a combination of the two. *Nephrol Dial Transplant* 23: 154–160, 2008. doi:10.1093/ndt/gfm661.
 34. Mogensen CE, Christensen CK, Vittinghus E. The stages in diabetic renal disease. With emphasis on the stage of incipient diabetic nephropathy. *Diabetes* 32: 64–78, 1983. doi:10.2337/diab.32.2.S64.
 35. Persson F, Rossing P. Diagnosis of diabetic kidney disease: state of the art and future perspective. *Kidney Int Suppl (2011)* 8: 2–7, 2018. doi:10.1016/j.kisu.2017.10.003.
 36. Nath KA. Tubulointerstitial changes as a major determinant in the progression of renal damage. *Am J Kidney Dis* 20: 1–17, 1992. doi:10.1016/s0272-6386(12)80312-x.
 37. Ichimura T, Bonventre JV, Bailly V, Wei H, Hession CA, Cate RL, Sanicola M. Kidney injury molecule-1 (KIM-1), a putative epithelial cell adhesion molecule containing a novel immunoglobulin domain, is up-regulated in renal cells after injury. *J Biol Chem* 273: 4135–4142, 1998. doi:10.1074/jbc.273.7.4135.
 38. Van Buren PN, Toto RD. The pathogenesis and management of hypertension in diabetic kidney disease. *Med Clin North Am* 97: 31–51, 2013. doi:10.1016/j.mcna.2012.10.003.
 39. Chow F, Ozols E, Nikolic-Paterson DJ, Atkins RC, Tesch GH. Macrophages in mouse type 2 diabetic nephropathy: correlation with diabetic state and progressive renal injury. *Kidney Int* 65: 116–128, 2004. doi:10.1111/j.1523-1755.2004.00367.x.
 40. Reidy K, Kang HM, Hostetter T, Susztak K. Molecular mechanisms of diabetic kidney disease. *J Clin Invest* 124: 2333–2340, 2014. doi:10.1172/JCI72271.
 41. Humphreys BD, Xu F, Sabbiseti V, Grgic I, Naini SM, Wang N, Chen G, Xiao S, Patel D, Henderson JM, Ichimura T, Mou S, Soeung S, McMahon AP, Kuchroo VK, Bonventre JV. Chronic epithelial kidney injury molecule-1 expression causes murine kidney fibrosis. *J Clin Invest* 123: 4023–4035, 2013. doi:10.1172/JCI45361.
 42. Brown NJ, Vaughan DE. Angiotensin-converting enzyme inhibitors. *Circulation* 97: 1411–1420, 1998. doi:10.1161/01.cir.97.14.1411.
 43. Binz-Lotter J, Jüngst C, Rinschen MM, Koehler S, Zentis P, Schauss A, Schermer B, Benzing T, Hackl MJ. Injured podocytes are sensitized to angiotensin II-induced calcium signaling. *J Am Soc Nephrol* 31: 532–542, 2020. doi:10.1681/ASN.2019020109.
 44. Ferrannini E, Mark M, Mayoux E. CV protection in the EMPA-REG OUTCOME trial: a thrifty substrate hypothesis. *Diabetes Care* 39: 1108–1114, 2016. doi:10.2337/dc16-0330.
 45. DeFronzo RA, Reeves WB, Awad AS. Pathophysiology of diabetic kidney disease: impact of SGLT2 inhibitors. *Nat Rev Nephrol* 17: 319–334, 2021. doi:10.1038/s41581-021-00393-8.
 46. Kidokoro K, Cherney DZI, Bozovic A, Nagasu H, Satoh M, Kanda E, Sasaki T, Kashihara N. Evaluation of glomerular hemodynamic function by empagliflozin in diabetic mice using in vivo imaging. *Circulation* 140: 303–315, 2019. doi:10.1161/CIRCULATIONAHA.118.037418.
 47. Tuttle KR, Brosius FC, Cavender MA, Fioretto P, Fowler KJ, Heerspink HJL, Manley T, McGuire DK, Molitch ME, Mottl AK, Perreault L, Rosas SE, Rossing P, Sola L, Vallon V, Wanner C, Perkovic V. SGLT2 inhibition for CKD and cardiovascular disease in type 2 diabetes: report of a scientific workshop sponsored by the National Kidney Foundation. *Diabetes* 70: 1–16, 2021. doi:10.2337/dbi20-0040.
 48. Gallo LA, Ward MS, Fotheringham AK, Zhuang A, Borg DJ, Flemming NB, Harvie BM, Kinneally TL, Yeh SM, McCarthy DA, Koepsell H, Vallon V, Pollock C, Panchapakesan U, Forbes JM. Once daily administration of the SGLT2 inhibitor, empagliflozin, attenuates markers of renal fibrosis without improving albuminuria in diabetic db/db mice. *Sci Rep* 6: 28124, 2016. doi:10.1038/srep28124.
 49. Cherney DZI, Perkins BA, Soleymanlou N, Maione M, Lai V, Lee A, Fagan NM, Woerle HJ, Johansen OE, Broedl UC, Von Eyntzen M. Renal hemodynamic effect of sodium-glucose cotransporter 2 inhibition in patients with type 1 diabetes mellitus. *Circulation* 129: 587–597, 2014. doi:10.1161/CIRCULATIONAHA.113.005081.
 50. Lambers Heerspink HJ, De Zeeuw D, Wie L, Leslie B, List J. Dapagliflozin a glucose-regulating drug with diuretic properties in subjects with type 2 diabetes. *Diabetes Obes Metab* 15: 853–862, 2013. doi:10.1111/dom.12127.
 51. Skrtic M, Cherney DZI. Sodium-glucose cotransporter-2 inhibition and the potential for renal protection in diabetic nephropathy. *Curr Opin Nephrol Hypertens* 24: 96–103, 2015. doi:10.1097/MNH.0000000000000084.
 52. Aroor AR, Das NA, Carpenter AJ, Habibi J, Jia G, Ramirez-Perez FI, Martinez-Lemus L, Manrique-Acevedo CM, Hayden MR, Duta C, Nistala R, Mayoux E, Padilla J, Chandrasekar B, DeMarco VG. Glycemic control by the SGLT2 inhibitor empagliflozin decreases aortic stiffness, renal resistivity index and kidney injury. *Cardiovasc Diabetol* 17: 108, 2018. doi:10.1186/s12933-018-0750-8.
 53. Eid SA, O'Brien PD, Hinder LM, Hayes JM, Mendelson FE, Zhang H, Zeng L, Kretzler K, Narayanan S, Abcouwer SF, Brosius FC, Pennathur S, Savelieff MG, Feldman EL. Differential effects of empagliflozin on microvascular complications in murine models of type 1 and type 2 diabetes. *Biology (Basel)* 9: 347–314, 2020. doi:10.3390/biology9110347.
 54. Nørgaard SA, Briand F, Sand FW, Galsgaard ED, Søndergaard H, Sørensen DB, Sulpice T. Nephropathy in diabetic db/db mice is accelerated by high protein diet and improved by the SGLT2 inhibitor dapagliflozin. *Eur J Pharmacol* 860: 172537, 2019. doi:10.1016/j.ejphar.2019.172537.
 55. Terami N, Ogawa D, Tachibana H, Hatanaka T, Wada J, Nakatsuka A, Eguchi J, Sato Horiguchi C, Nishii N, Yamada H, Takei K, Makino H. Long-term treatment with the sodium glucose cotransporter 2 inhibitor, dapagliflozin, ameliorates glucose homeostasis and diabetic nephropathy in db/db mice. *PLoS One* 9: e100777, 2014. doi:10.1371/journal.pone.0100777.
 56. Tomita I, Kume S, Sugahara S, Osawa N, Yamahara K, Yasuda-Yamahara M, Takeda N, Chin-Kanasaki M, Kaneko T, Mayoux E, Mark M, Yanagita M, Ogita H, Araki S, I, Maegawa H. SGLT2 inhibition mediates protection from diabetic kidney disease by promoting ketone body-induced mTORC1 inhibition. *Cell Metab* 32: 404–419.e6, 2020. doi:10.1016/j.cmet.2020.06.020.
 57. Castoldi G, Carletti R, Ippolito S, Colzani M, Barzaghi F, Stella A, Zerbini G, Perseghin G, Di Gioia CRT. Renal anti-fibrotic effect of sodium glucose cotransporter 2 inhibition in angiotensin II-dependent hypertension. *Am J Nephrol* 51: 119–129, 2020. doi:10.1159/000505144.

58. **Reyes-Pardo H, Bautista R, Vargas-Robles H, Rios A, Sánchez D, Escalante B.** Role of sodium/glucose cotransporter inhibition on a rat model of angiotensin II-dependent kidney damage. *BMC Nephrol* 20: 292, 2019. doi:[10.1186/s12882-019-1490-z](https://doi.org/10.1186/s12882-019-1490-z).
59. **Zhang Y, Thai K, Kepecs DM, Gilbert RE.** Sodium-glucose linked cotransporter-2 inhibition does not attenuate disease progression in the rat remnant kidney model of chronic kidney disease. *PLoS One* 11: e0144640, 2016. doi:[10.1371/journal.pone.0144640](https://doi.org/10.1371/journal.pone.0144640).
60. **Miyata KN, Lo C-S, Zhao S, Liao M-C, Pang Y, Chang S-Y, Peng J, Kretzler M, Filep JG, Ingelfinger JR, Zhang S-L, Chan JSD.** Angiotensin II up-regulates sodium-glucose co-transporter 2 expression and SGLT2 inhibitor attenuates Ang II-induced hypertensive renal injury in mice. *Clin Sci* 135: 943–961, 2021. doi:[10.1042/CS20210094](https://doi.org/10.1042/CS20210094).
61. **Lin B, Koibuchi N, Hasegawa Y, Sueta D, Toyama K, Uekawa K, Ma MJ, Nakagawa T, Kusaka H, Kim-Mitsuyama S.** Glycemic control with empagliflozin, a novel selective SGLT2 inhibitor, ameliorates cardiovascular injury and cognitive dysfunction in obese and type 2 diabetic mice. *Cardiovasc Diabetol* 13: 148, 2014. doi:[10.1186/s12933-014-0148-1](https://doi.org/10.1186/s12933-014-0148-1).
62. **Dalbøge LS, Almholt DLC, Neerup TSR, Vassiliadis E, Vrang N, Pedersen L, Fosgerau K, Jelsing J.** Characterisation of age-dependent beta cell dynamics in the male db/db mice. *PLoS One* 8: e82813, 2013. doi:[10.1371/journal.pone.0082813](https://doi.org/10.1371/journal.pone.0082813).